Hindawi
Advances in Civil Engineering
Volume 2023, Article ID 8210239, 10 pages
https://doi.org/10.1155/2023/8210239

Research Article

CDEM-Based Numerical Simulation of Uniaxial Compressive Mechanical Properties of Rocks

Mingming Liu,[1,2] **Zhiyong Song**,[1] **Shou Ma**,[2] **Yuhua Wei**,[2] **and Jingrui Wang**[2]

[1]*School of Civil and Resource Engineering, University of Science and Technology Beijing, Beijing 100083, China*
[2]*SinoFTS Petroleum Services Ltd., Sinopec Huadong Oilfield Service Corporation, Beijing 100101, China*

Correspondence should be addressed to Mingming Liu; mingming.liu@sinofts.com

Received 23 August 2023; Revised 28 November 2023; Accepted 2 December 2023; Published 27 December 2023

Academic Editor: Tianshou Ma

Understanding the mechanical properties of rock is of great significance for the development of unconventional reservoirs. However, a large number of bedding makes the mechanical laws of rock unclear. To investigate the effect of bedding properties on the uniaxial mechanical properties of rock, the coal model containing bedding is developed based on the continuous–discontinuous method, and the effect of bedding angle, bedding strength, bedding number, and loading rate on the uniaxial mechanical properties of rock is investigated. The failure morphology, stress–strain evolution, peak stress, and fracture degrees are analyzed and discussed in detail. The reliability of the numerical model in this paper has been verified by comparison with the indoor experiments. The results show that when the bedding angle is 0°, the peak stress of the rock is maximum, 8.16 MPa, and when the bedding angle is 90°, the fracture degree of the rock is maximum, 3.74%. For the different bedding strengths, the peak stress first decreases linearly with the decrease of the bedding strength. The peak stress barely varies when the bedding strength is less than 0.5 MPa. The fracture degree of the rock shows a nonlinear increase with the increase in bedding strength. For different bedding numbers, the activation of the bedding is not related to the bedding number. The loading speed also has a great influence on the mechanical properties of rock. With the increase in loading rate, the difficulty of bedding activation gradually increases, and the complexity of fractures gradually increases. This study aims to further improve the understanding of the effect of bedding properties on the uniaxial mechanical properties of rock.

1. Introduction

Coalbed methane is gradually developing as an important energy resource in unconventional oil and gas [1–3]. Hydraulic fracturing as an effective means to increase reservoir permeability has been widely used in the process of coalbed methane production [3–6]. However, the coal contains a large number of bedding, microfractures, and other defects, which often makes the hydraulic fracture propagation pattern unclear [7–9]. Therefore, it is significant to clarify the effect of bedding on the mechanical properties of coal for hydraulic fracturing [10–14].

The mechanical properties of coal have attracted numerous scholars to investigate [15–19]. Zagorščak and Thomas [20] investigated the effect of subcritical and supercritical carbon dioxide saturation on uniaxial compressive damage and elastic deformation of high-order coals. Grgic et al. [15] determined the dynamic stiffness tensor and velocity anisotropy during uniaxial loading by experiment, and the effect of water content on mechanical properties was evaluated. Tang et al. [21] discussed the energy evolution during uniaxial and triaxial compression of coal. In addition, the effects of coal rank, loading pressure, temperature, loading direction, and other factors have been widely investigated. The properties of bedding also have a great influence on the mechanical properties of coal, but less relevant research has been conducted [22–24]. Li et al. [25] investigated the effects of loading direction on failure load test results for Brazilian tests on coal rock. Cheng et al. [26] investigated the effect of bedding distribution on the strength and failure strength of coal under uniaxial compression by using COMSOL and MATLAB. Zhao et al. [27] investigated the anisotropy of coal under uniaxial compression by experimental and numerical methods, and the results showed that the strength anisotropy of coal is influenced by the directional distribution of the microstructure. Wang et al. [28] investigated in detail the scaling effect, the relationship between

damage mode and stress–strain behavior, and the main reasons for the fluctuation of stress–strain curves in the uniaxial compressive strength of coal rocks with T-shaped joints. The above studies often neglect the influence of the properties of the bedding on the mechanical properties of coal [29]. Therefore, it is important to further investigate the understanding of the influence of bedding properties (angle, strength, density, etc.) on the mechanical properties of coal rocks in detail. Some traditional numerical models are developed to study the problem but still face some limitations, e.g., finite element method meshes cannot be easily changed after creation and require further assumptions and simplifications, and discrete element models have advantages in modeling discontinuous problems but require access to many fundamental data which are often unavailable. Therefore, to fully combine the advantages of finite element and discrete element methods, the continuum–discontinuum method is developed and has achieved good performance [30].

This paper aims to investigate the effect of bedding properties on the uniaxial mechanical properties of coal by the continuous–discontinuous method. The four factors of bedding angle, bedding strength, bedding number, and loading rate are considered comprehensively, and the rock failure pattern, stress–strain evolution law, peak strength, and rock failure degree are analyzed in detail. The results are significant for the reunderstanding of the mechanical properties of coal with bedding.

2. Mathematical and Physical Models

The continuous–discontinuous method is a dynamic explicit solution algorithm that combines the advantages of finite element and discrete element algorithms, and this method can simulate the whole process of initiation, extension, and failure of continuous material. The numerical model consists of two parts: the block and the interface. The block is used to characterize the elasticity, plasticity, and damage of the material, while the interface is used to characterize discontinuous features such as fracture and slip. The explicit Eulerian front differential method based on the incremental approach is adopted to solve the dynamic problem, which mainly contains two parts: nodal joint force calculation and nodal motion calculation, as shown in Equations (1) and (2).

$$F = F^E + F^e + F^c + F^d, \tag{1}$$

where F is the total nodal force, N; F^E is the nodal external force, N; F^e is the nodal force contributed by the element deformation, N; is the nodal force contributed by the contact interface, N; and F^d is the nodal damping force, N.

$$\left\{ \begin{array}{c} a = \dfrac{F}{m}, v = \sum_{t=0}^{T_{\text{now}}} a\Delta t \\ \Delta u = v\Delta t, u = \sum_{t=0}^{T_{\text{now}}} \Delta u \end{array} \right\}, \tag{2}$$

where a is the node acceleration, m^2/s; v is the node velocity, m/s; u is the node displacement, m; Δu is the node displacement increment, m; m is the nodal mass, kg; Δt is the time step, s.

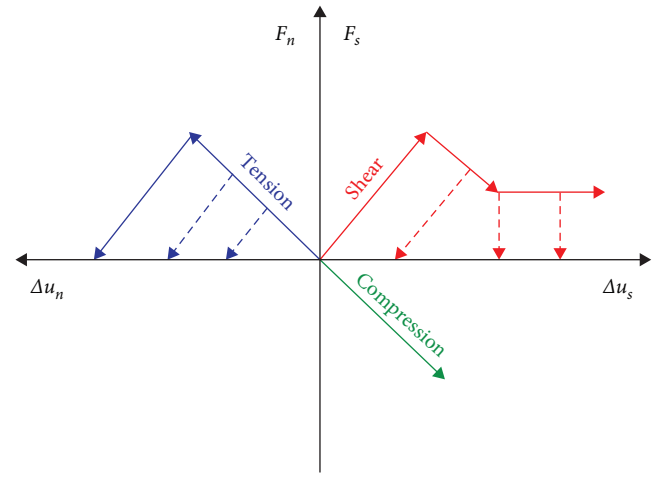

Figure 1: The normal and tangential intrinsic curves of the interface.

The elastic constitutive of the element represented by the incremental method is given by Equation (3).

$$\left\{ \begin{array}{c} \Delta\sigma_{ij} = 2G\Delta\varepsilon_{ij} + \left(K - \dfrac{2}{3}G\right)\Delta\theta\delta_{ij} \\ \sigma_{ij}(t_1) = \Delta\sigma_{ij} + \sigma_{ij}(t_0) \end{array} \right\}, \tag{3}$$

where is the stress tensor increment, MPa; σ_{ij} is the stress tensor, MPa; G is the shear modulus, MPa; $\Delta\varepsilon_{ij}$ is the strain tensor increment, K is the bulk modulus, MPa; $\Delta\theta$ is the body strain increment, δ_{ij} is the Kronecker notation, t_1 is the next time step, and t_0 is the current time step.

The maximum tensile stress criterion and the Coulombs–Moore criterion are adopted in this paper to conduct the calculation of damage and fracture, as shown in Equations (4) and (5). The normal and tangential intrinsic curves of the interface are shown in Figure 1.

$$\sigma_n \geq T, \tag{4}$$

where σ_n is the normal stress, MPa; and T is the tensile strength MPa.

$$\sigma_t > c + \sigma_n \tan\varphi, \tag{5}$$

where σ_t is the tangential stress, MPa; c is the cohesion, MPa; and φ is the internal friction angle, degree.

To investigate the effect of different bedding properties on the uniaxial mechanical properties of coal, the standard core model with different bedding angles (0°, 30°, 45°, 60°, 90°) is developed in this paper. The model size is 25 mm × 50 mm, and the model is meshed by Gmsh software with 1 mm mesh size and triangular mesh type. The bedding is predefined by the hardline method with a bedding spacing of 12.5 mm. Two rigid surfaces are set up in the upper and lower parts of

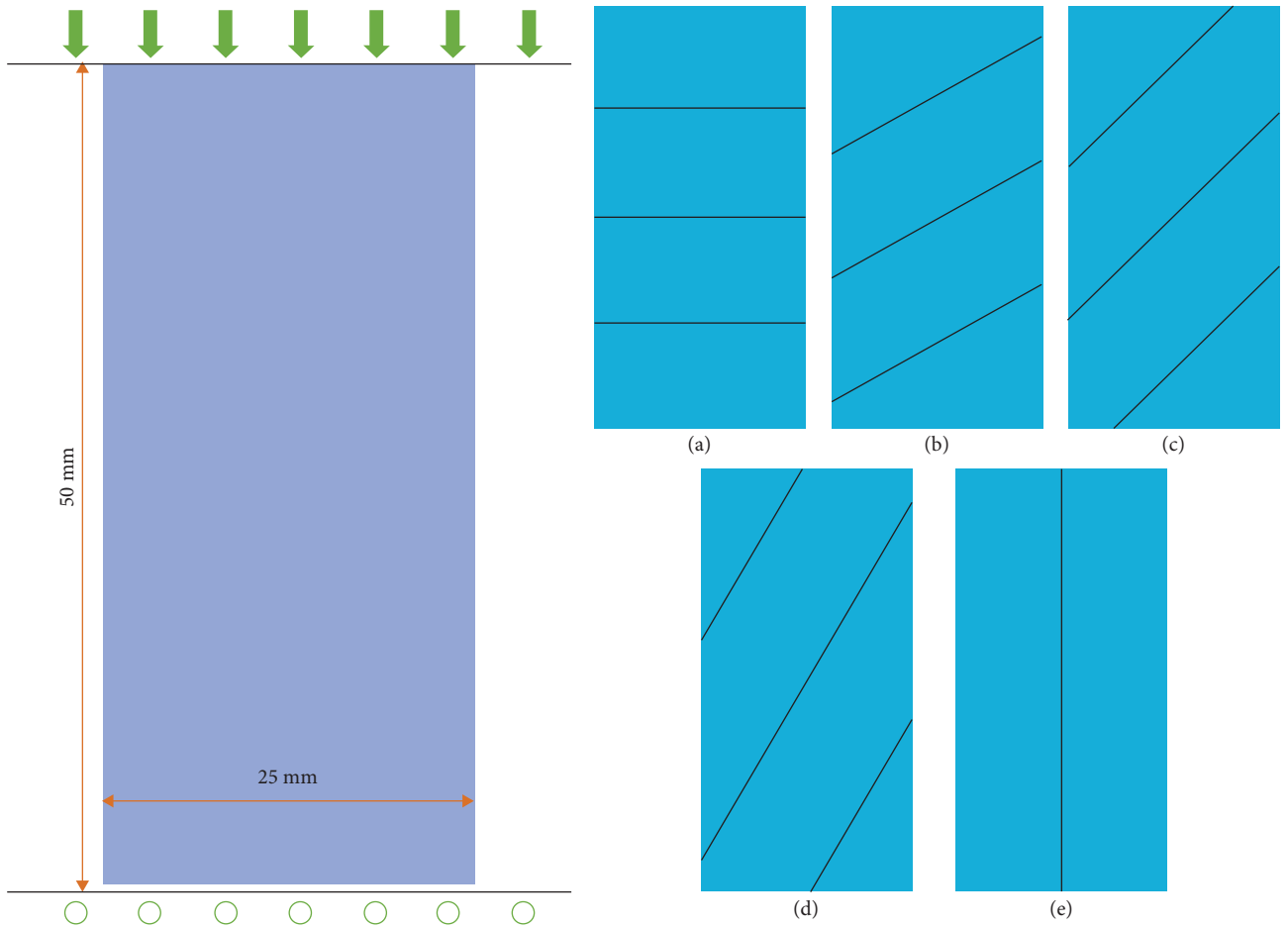

Figure 2: The coal model schematic: (a) 0°; (b) 30°; (c) 45°; (d) 60°; (e) 90°.

Table 1: The rock matrix material parameters.

Parameter	Value	Unit	Parameter	Value	Unit
Density	1,300	kg/m^3	Tensile strength	6	GPa
Elastic modulus	3	GPa	Cohesion	6	GPa
Poisson	0.3	–	Internal friction angle	40	Degree

Table 2: The rock material parameters for validation models.

Parameter	Value	Unit	Parameter	Value	Unit
Density	1,390	kg/m^3	Tensile strength	8	GPa
Elastic modulus	9	GPa	Cohesion	8	GPa
Poisson	0.34	–	Internal friction angle	30	Degree

the coal, respectively. The displacement constraint at the bottom and the displacement loading at the top of the coal are adopted to realize the simulation of rock uniaxial loading, and the model schematic is shown in Figure 2. The rock matrix strength is set to 30 times the bedding strength to reflect the weak cementation property of the bedding, and the rock matrix material parameters are shown in Table 1.

3. Model Validation

To verify the reliability of the numerical calculation model, the uniaxial mechanical experiments of coal by Cheng et al. [26] are compared with the numerical simulation results of the homogeneous model, and the rock material parameters are shown in Table 2. The model size is 50 mm × 100 mm, and both tests are conducted by displacement loading. The

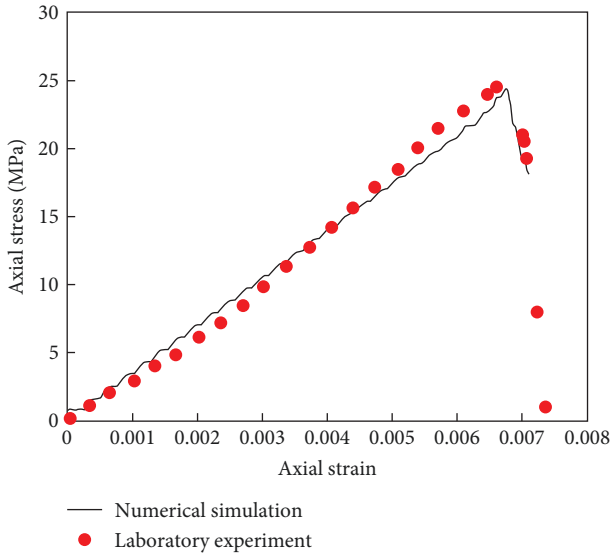

Figure 3: The comparison of the stress–strain curves between experimental and numerical simulation.

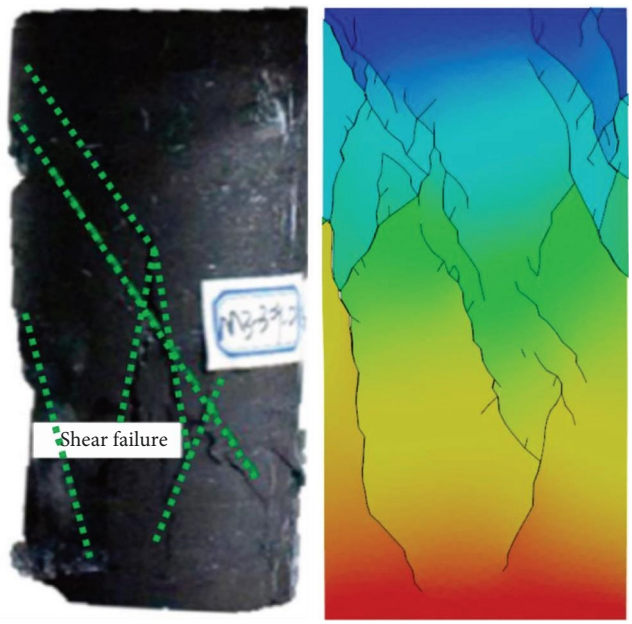

Figure 4: The fracture morphology of the experimental and numerical simulation.

trial-and-error method is used to calibrate the physical parameters of the numerical model. Figure 3 shows the comparison of the stress–strain curves between the laboratory experimental and the numerical simulation. The results show that the simulated results are consistent with experimental results; the uniaxial peak strengths for the experimental and numerical simulation are 24.82 and 24.41 MPa, respectively, with a relative error of 1.6%. Figure 4 shows the fracture morphology of the experimental and numerical simulations and the results show that the distribution locations of the main fractures are the same between the experimental and numerical simulations. Therefore, the reliability

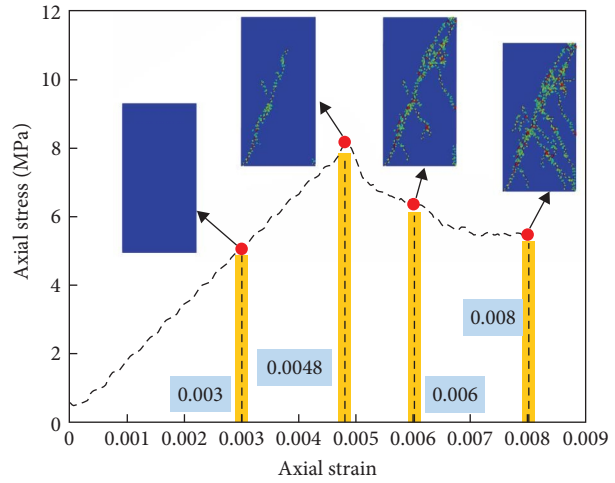

Figure 5: The fracture morphology and stress–strain evolution relationship at 0° of bedding angle.

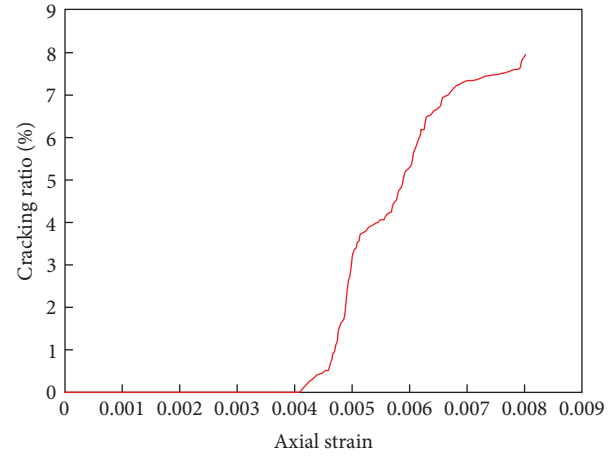

Figure 6: The evolution relationship of the fracture degree with axial strain.

of the numerical model in this paper is verified by the comparison results of stress–strain curves and fracture morphology.

4. The Effect of Bedding Angle

The fracture morphology and stress–strain evolution law at 0° of the bedding angle are shown in Figure 5. At the initial stage of loading, the rock is compressed and deformed, and the internal stress gradually accumulates, but it has not reached the critical damage state of the rock, so there is no fracture occurred. As the load increases, the rock satisfies the damage criterion, and breaking down occurs. A main fracture is initiated, and the internal stress in the rock reaches its maximum (peak stress). When the strain reached 0.006, the fracture began to propagate around the main fracture and formed the branch fracture. When the strain reaches 0.008, the fracture further propagation, and finally a one-sided fracture with 45° as the dividing line is formed at the end of loading.

Figure 6 shows the evolution relationship of the fracture degree with axial strain. The fracture degree is the ratio of the

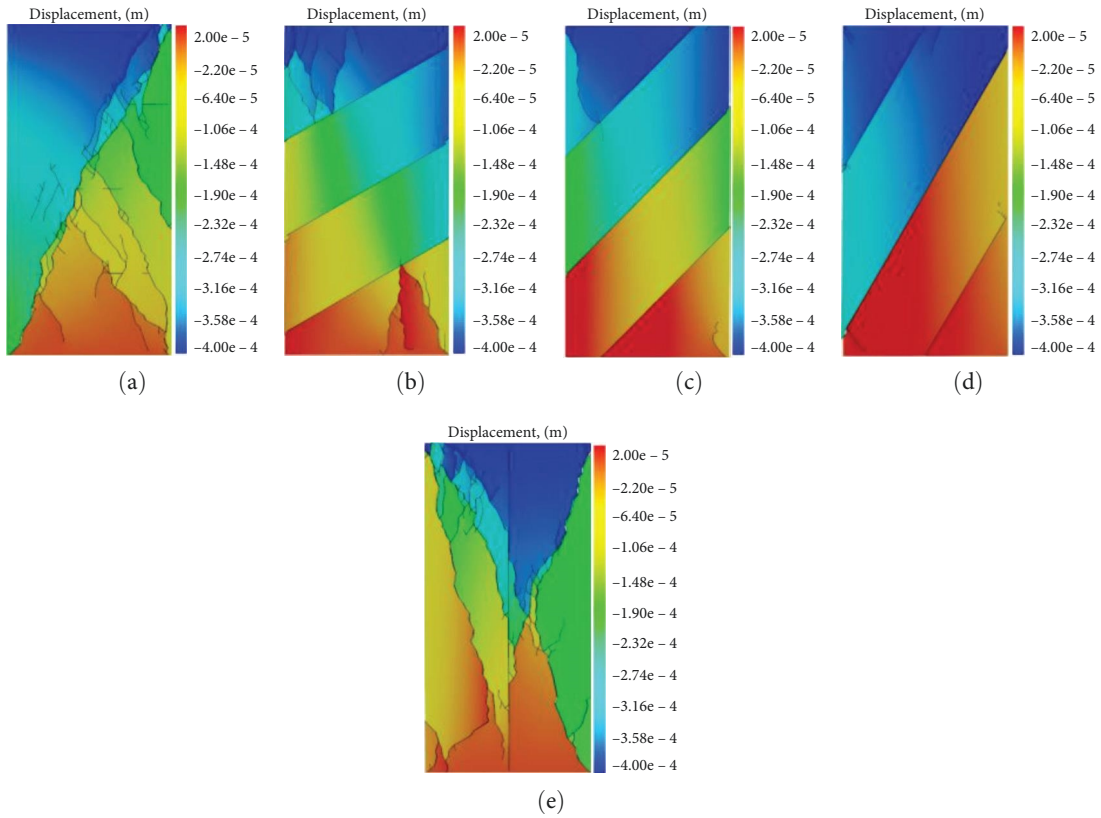

Figure 7: The fracture morphology at different bedding angles: (a) 0°; (b) 30°; (c) 45°; (d) 60°; (e) 90°.

area of the damaged elements to the total area of the total elements. Before the strain of 0.00408, the rock is not damaged by the strength of the rock itself, and the fracture degree is 0. As the loading proceeds, the internal stress of the rock gradually increases and reaches the failure threshold of the rock, and the rock fracture degree gradually increases. The evolution of rock fracture degree can be divided into three stages. In the first stage, the strain is 0.00408–0.00458. This stage is the initiation stage of fracture, and a small amount of fractures gradually appear in the rock. The second stage is the strain of 0.00458–0.00554, and this stage is the formed stage of the main fracture. The rock strength gradually reaches the maximum value and decreases rapidly in this stage. The third stage is the strain of 0.00554–0.008, and the stage is the branching fracture formation stage; the main fracture changes the stress distribution state of the rock, causing a large number of branching fractures to form around the main fracture. In addition, all three stages gradually slow down in the rate of fracture formation at the end of the stage, indicating that the damage inside the rock is a process of continuous accumulation and release of energy. There are differences in the energy accumulated at different stages, leading to differences in the complexity of the fractures.

The fracture morphology at different bedding angles (0°, 30°, 45°, 60°, 90°) are shown in Figure 7. The results showed that the bedding is fully activated at all angles except for the bedding angle of 0°. A few bedding are activated at 0°, a 45° main fracture is formed in the rock, and several branching fractures are formed around the main fracture. A branching

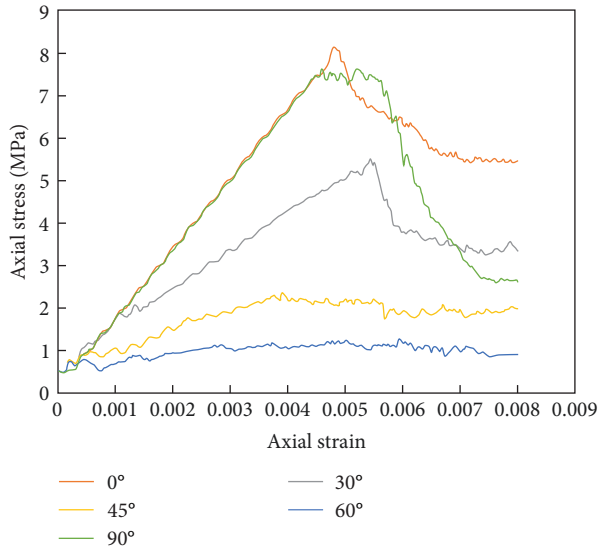

Figure 8: The stress–strain evolution curves at different bedding angles.

fracture is formed at the ends of the rock at 45°. There is almost no new fracture formation at 60°, except for bedding. At 90°, in addition to the bedding being activated, multiple main fractures are formed inside the rock, and the fracture morphology is more complicated.

Figure 8 shows the stress–strain evolution curves at different bedding angles. For 0° bedding, the stress–strain

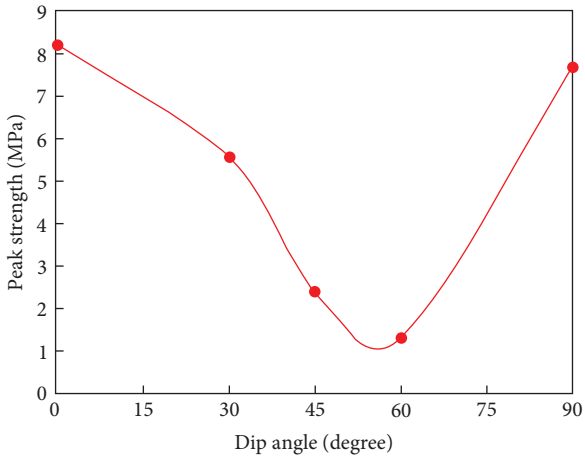

Figure 9: The peak stress of the rock at different bedding angles.

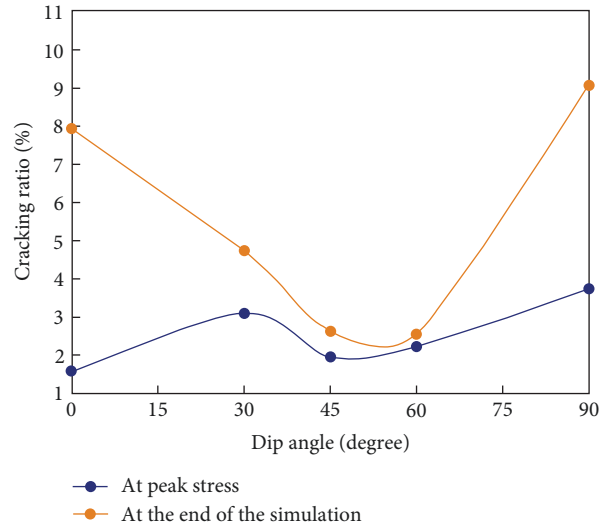

Figure 10: The rock fracture degree for different bedding angles.

showed a linear relationship before the peak stress and decreased rapidly after reaching the peak stress, showing the brittle failure characteristics. For 30° bedding, the peak stress decreases, and the corresponding peak strain is delayed. At 45° bedding, the peak strength further decreases, and the peak strain further increases; in addition, the failure stage is not obvious. At 60° bedding, there is no obvious peak, and the stress drop is not obvious. The 90° bedding is more similar to the 0° bedding before the peak. The 90° bedding stabilizes for a longer time when entering the peak stage, and the brittle failure characteristics are more obvious. In addition, it can be found that the larger the area of the stress–strain integration before the peak, the more obvious the failure characteristics and the more complex the fracture morphology. The greater the energy accumulated in the early stage, the greater the rate of energy release in the later stage, and the more conducive to the formation of complex fractures.

The peak stress of the rock at different bedding angles is shown in Figure 9. The results show that the peak stress of the coal shows a "V" pattern with the increase of the bedding angle, and the maximum values are reached at 0° and 90°, 8.16 and 7.65 MPa, respectively, and the minimum values are reached at 60°, 1.29 MPa.

Figure 10 shows the rock fracture degree at the peak stress and at the end moment of loading for different bedding angles. The results show that at the peak stress, the fracture degree at different bedding angles shows the "N" pattern; the maximum value of 3.74% is obtained at 90°, and the minimum value of 1.58% is obtained at 0°. At the end of loading, the fracture degree at different bedding angles showed the "V" pattern, with a maximum value of 9.07% at 90° and smaller values of 2.64% at 60°. Therefore, when the loading direction is parallel to the bedding direction, it is conducive to the formation of complex fractures, and when the loading direction is perpendicular to the bedding, the fracture generation mainly occurs in the postpeak stage. When the loading direction is at other angles to the bedding, the difference in the number of fractures from pre- to postpeak is relatively small because of the shear slip of the bedding.

5. The Effect of Bedding Strength

To investigate the effects of different bedding strengths on the uniaxial mechanical properties of coal, five different bedding strengths, 0, 0.1, 0.5, 1, and 2 MPa, are set on the 30° bedding model. Figure 11 shows the schematic diagram of the fracture morphology at different bedding strengths. The results show that the bedding is not fully activated at 2 MPa bedding strength, and more branching fractures and microfractures are formed at 1 MPa bedding strength. The bedding is fully activated, and a main fracture that crosses the bedding and some branching fractures are formed around the main fracture. The bedding is fully activated at 0.5 MPa and some microfractures appeared at the rock ends. When the bedding strength decreases to 0.1 and 0 MPa, the bedding is all fully activated, but the branch fractures or microfractures are gradually decreased.

Figure 12 shows the stress–strain evolution relationship for different bedding strengths. The results show that different bedding strengths all show the characteristics of brittle failure, and the peak stress of the rock increases with the increase of bedding strength. The stress–strain curve shows the double-peaked feature at 1 MPa, mainly related to the activation of the bedding and the formation of the main fracture, the formation of two larger fractures, causing the stress to release and reaccumulate more quickly. When the bedding strength is less than 0.5 MPa, the difference between the stress–strain curves gradually decreases.

Figure 13 shows the peak stress and fracture degree of coal at different bedding strengths. The results show that the peak stress increases with the increase of bedding strength, and the maximum peak stress is 7.81 MPa at 2 MPa bedding strength. When the bedding strength is less than 0.5 MPa, the peak stress gradually stabilizes at 5.51 MPa. The rock fracture degree gradually increases with the increase of bedding strength, but the increase rate gradually increases. It can be found that there is a positive correlation between the rock fracture degree and the peak stress.

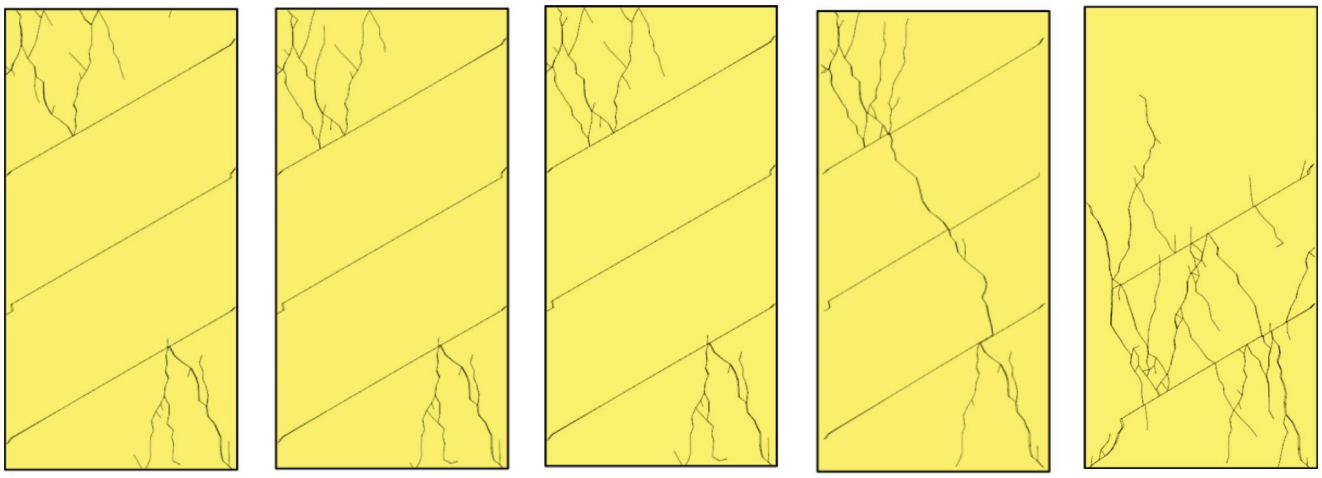

Figure 11: The schematic diagram of the fracture morphology at different bedding strengths: (a) 0 MPa; (b) 0.1 MPa; (c) 0.5 MPa; (d) 1 MPa; (e) 2 MPa.

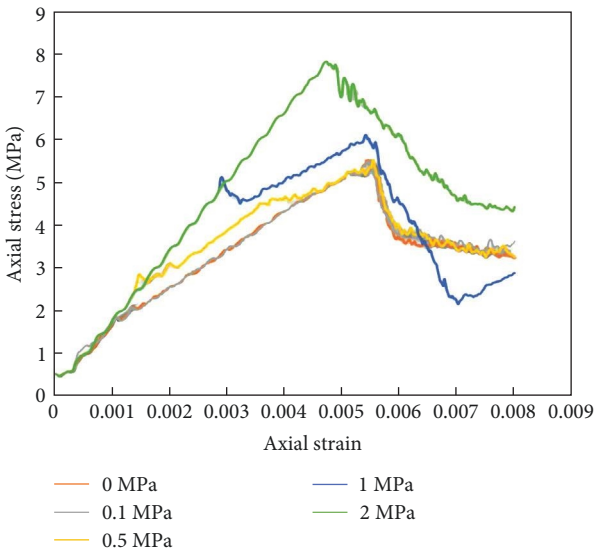

Figure 12: The stress–strain evolution relationship for different bedding strengths.

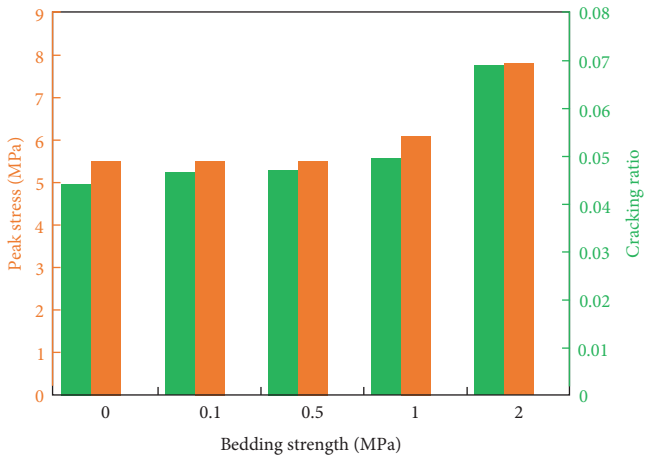

Figure 13: The peak stress and fracture degree of coal at different bedding strengths.

6. The Effect of Bedding Number

To investigate the effect of the number of bedding on the uniaxial mechanical properties of coal, five rock models with different numbers of bedding (1, 2, 3, 4, and 5) are set up based on the 45° bedding model. Figure 14 shows the schematic diagram of the fracture morphology with different numbers of bedding. The results show that the bedding under different models is fully activated. Therefore, the activation of bedding is independent of the number of bedding. When one bedding is present, in addition to the bedding being activated, a fracture is formed at the end of the rock. When two beddings existed, the stress concentration caused more microcracks to form around the end of rock. With the further increase in the number of bedding, the formation of fractures within the bedding becomes more difficult.

Figure 15 shows the stress–strain evolution relationship for different numbers of bedding. Since the shear slip of the bedding causes a large stress concentration at the end when there are two beddings, the stress increases fastest, and the peak stress is the largest, with obvious brittle damage characteristics. When there is one bedding, the stress increases more slowly, and the peak stress decreases relatively. The stress–strain evolution pattern is more similar for other bedding models (3, 4, and 5), and their fracture morphologies are also more similar.

Figure 16 shows the peak stress and fracture degree of coal for different numbers of bedding. The results show that the maximum peak stress is 4.71 MPa when there are two beddings. The peak stress gradually decreases with the increase in the number of bedding. The rock fracture degree is at its maximum (3.39%) when there are five beddings. With the increase of the number of beddings except for two beddings, the rock fracture degree gradually decreases, and it is consistent with the evolution of the peak stress of the rock.

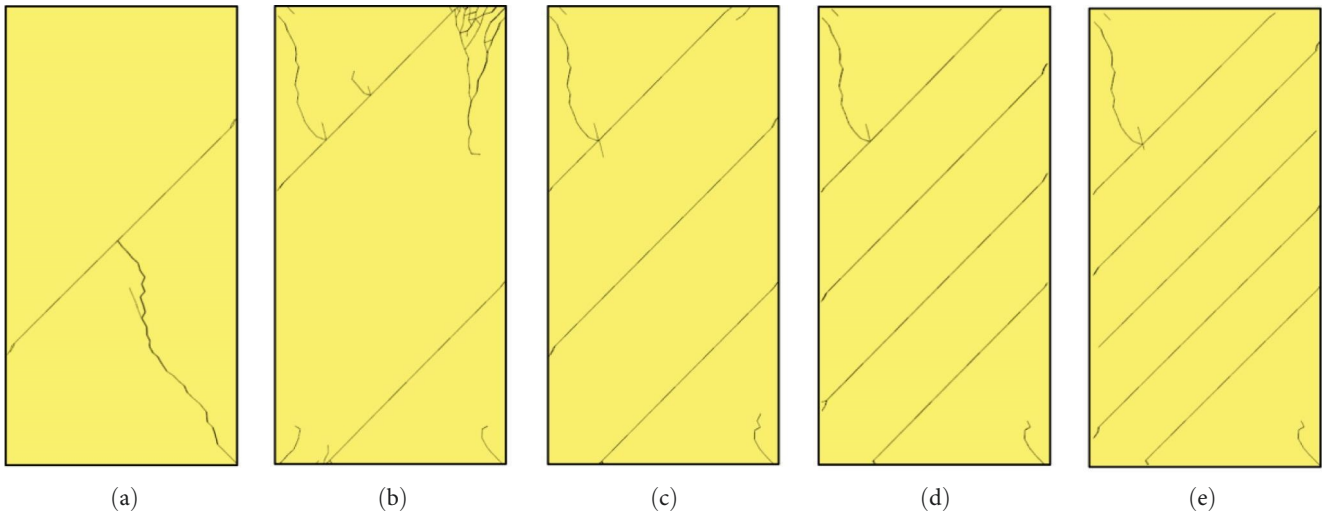

Figure 14: The schematic diagram of the fracture morphology with different numbers of bedding: (a) 1; (b) 2; (c) 3; (d) 4; (e) 5.

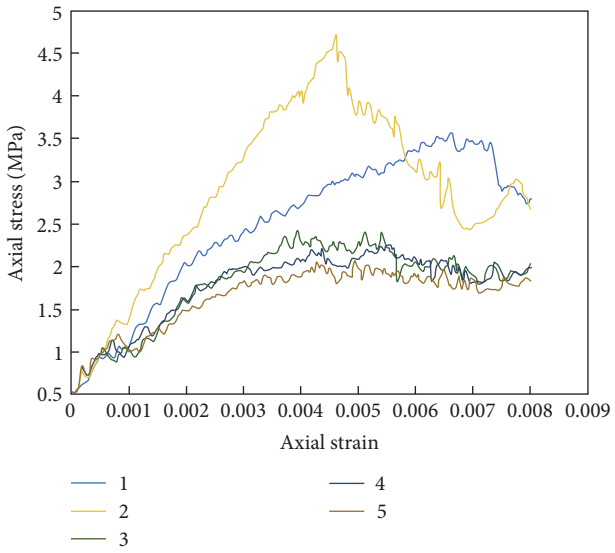

Figure 15: The stress–strain evolution relationship for different numbers of bedding.

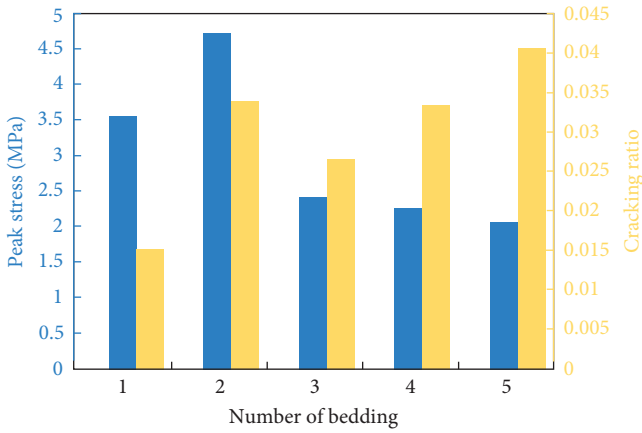

Figure 16: The peak stress and fracture degree of coal for different numbers of bedding.

7. The Effect of Loading Rate

To investigate the effects of different loading rates on the uniaxial mechanical properties of coal, five different loading velocities, 5e–9 m/s, 1e–8 m/s, 2e–2 m/s, 4e–8 m/s, and 8e–8 m/s, are set on the 90° bedding model. Figure 17 shows the fracture morphology at different loading rates. The results show that the difficulty of bedding activation gradually increases with the increase in loading speed, and the complexity of fractures gradually increases.

Figure 18 shows the stress–strain evolution relationship for different loading rates. The results show that the stress–strain difference between different loading rates is small before the peak. The peak stress of the rock increases with the increase of the loading rate, and the peak strain also increases. On the other hand, the number of microcracks gradually increases with increasing loading velocity, causing the brittle characteristics to gradually become less obvious.

Figure 19 shows the peak stress and the fracture ratio of coal for different loading rates. The results show that there is a positive correlation between the loading rate and the peak stress. The peak stress increases gradually with the loading rate being higher, and the rate of increase gradually decreases. The results of the rock fracture degree show that the loading rate is conducive to increasing the rock fracture degree, and the fracture degree reaches the maximum value of 12.5% at 8e–8 m/s. With the decrease in loading rate, the rock fracture degree also shows a decreasing trend.

8. Conclusion

(1) The bedding angle has a great effect on the uniaxial mechanical properties of coal. The physical properties of different bedding angles are symmetrically similar, with 90° as the dividing line. The maximum peak stress is 8.16 MPa at a 0° bedding angle, and the

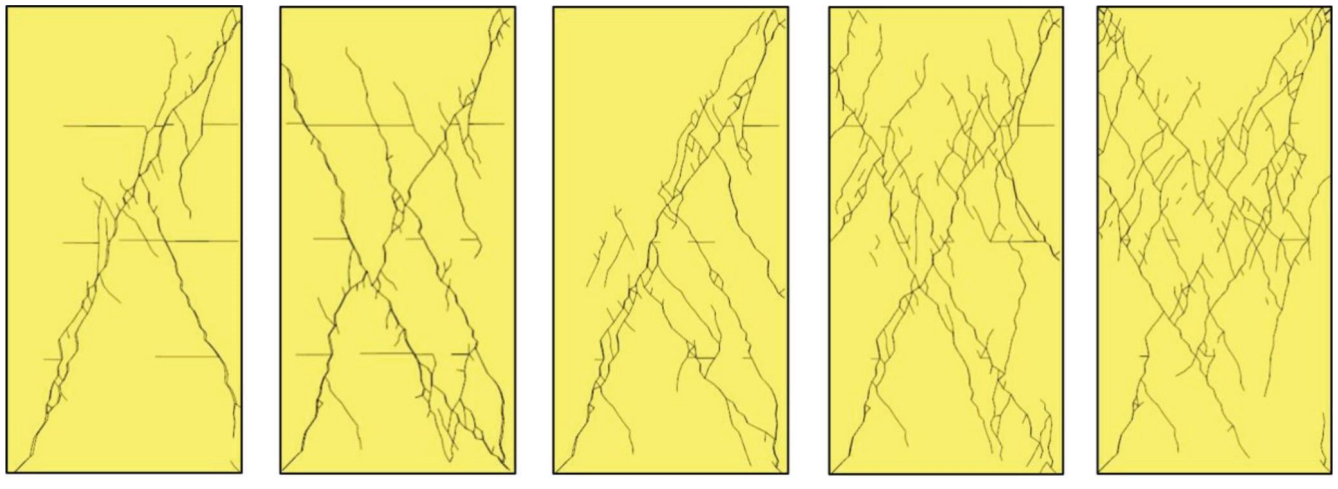

Figure 17: The fracture morphology at different loading rates: (a) 5e–9 m/s; (b) 1e–8 m/s; (c) 2e–8 m/s; (d) 4e–8 m/s; (e) 8e–8 m/s.

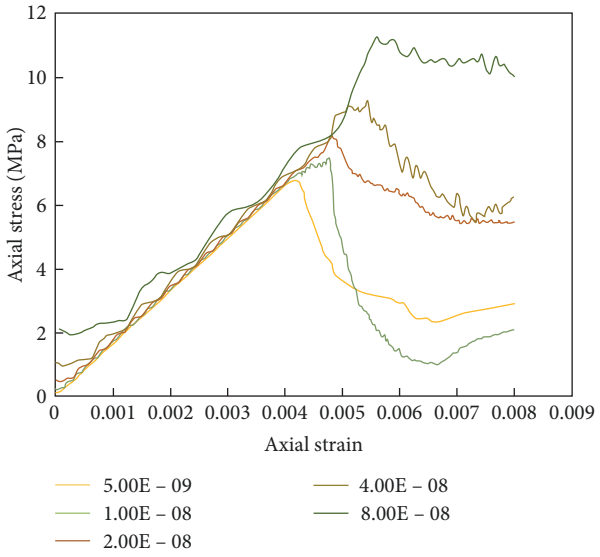

Figure 18: The stress–strain evolution relationship for different loading rates.

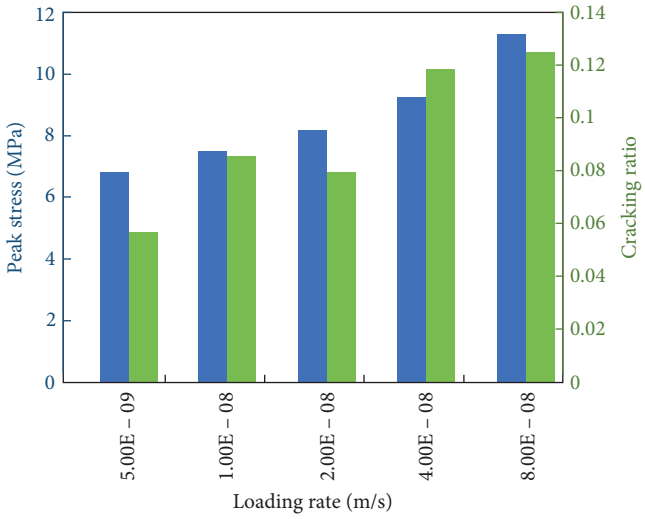

Figure 19: The peak stress and the fracture ratio of coal for different loading rates.

maximum rock fracture ratio is 3.74% at a 90° bedding angle.

(2) The peak stress decreases in a linear proportion with the decrease in the bedding strength. When the bedding strength is less than 0.5 MPa, the peak rock stress does not change and is 5.51 MPa.

(3) The activation of bedding is independent of the number of bedding. In addition, the loading speed also has a great influence on the mechanical properties of coal; with the increase in loading speed, the difficulty of bedding activation gradually increases, but the complexity of fractures gradually increases.

Data Availability

The authors confirm that the data supporting the findings of this study are available in the article.

Conflicts of Interest

The authors declare that there are no conflicts of interest.

References

[1] L. Hou, X. Liu, L. Liang et al., "Investigation of coal and rock geo-mechanical properties evaluation based on the fracture complexity and wave velocity," *Journal of Natural Gas Science and Engineering*, vol. 75, Article ID 103133, 2020.

[2] Z. Moradian, A. Seiphoori, and B. Evans, "The role of bedding planes on fracture behavior and acoustic emission response of shale under unconfined compression," in *51st U.S. Rock Mechanics/Geomechanics Symposium*, OnePetro, San Francisco, California, USA, 2017.

[3] H. Wang, T. Ma, Y. Liu, B. Wu, and P. G. Ranjith, "Numerical and experimental investigation of the anisotropic tensile behavior of layered rocks in 3D space under Brazilian test conditions," *International Journal of Rock Mechanics and Mining Sciences*, vol. 170, Article ID 105558, 2023.

[4] G. Huang, X. Hu, F. Zhou, X. Li, E. Dong, and Z. Li, "A new multi-cluster fracturing simulation model coupled with perforation erosion: based on the continuous–discontinuous method,"

Rock Mechanics and Rock Engineering, vol. 56, pp. 3887–3901, 2023.

[5] T. A. Moore, "Coalbed methane: a review," *International Journal of Coal Geology*, vol. 101, pp. 36–81, 2012.

[6] Q. Shi, Y. Qin, J. Li, Z. Wang, M. Zhang, and X. Song, "Simulation of the crack development in coal without confining stress under ultrasonic wave treatment," *Fuel*, vol. 205, pp. 222–231, 2017.

[7] Y. Li, M. Long, L. Zuo, W. Li, and W. Zhao, "Brittleness evaluation of coal based on statistical damage and energy evolution theory," *Journal of Petroleum Science and Engineering*, vol. 172, pp. 753–763, 2019.

[8] S. Lyu, S. Wang, X. Chen et al., "Natural fractures in soft coal seams and their effect on hydraulic fracture propagation: a field study," *Journal of Petroleum Science and Engineering*, vol. 192, Article ID 107255, 2020.

[9] Y. Zhao, G.-F. Zhao, Y. Jiang, D. Elsworth, and Y. Huang, "Effects of bedding on the dynamic indirect tensile strength of coal: laboratory experiments and numerical simulation," *International Journal of Coal Geology*, vol. 132, pp. 81–93, 2014.

[10] S. Gong, Z. Wang, L. Zhou, and H. Ding, "Dynamic fracture mechanics and energy distribution rate response characteristics of coal containing bedding structure," *PLOS ONE*, vol. 16, no. 6, Article ID e0247908, 2021.

[11] Q. Ma, X. Liu, Y. Tan et al., "Numerical study of mechanical properties and microcrack evolution of double-layer composite rock specimens with fissures under uniaxial compression," *Engineering Fracture Mechanics*, vol. 289, Article ID 109403, 2023.

[12] T. Ma, H. Wang, Y. Liu, C. Fu, and P. G. Ranjith, "Experimental investigation on the anisotropy of mode-I fracture and tensile failure of layered shale," *Engineering Fracture Mechanics*, vol. 290, Article ID 109484, 2023.

[13] S.-Q. Yang, W.-L. Tian, P. G. Ranjith, X.-R. Liu, M. Chen, and W. Cai, "Three-dimensional failure behavior and cracking mechanism of rectangular solid sandstone containing a single fissure under triaxial compression," *Rock Mechanics Bulletin*, vol. 1, no. 1, Article ID 100008, 2022.

[14] Q. Zhang, Z. Zhi, C. Feng, R. Li, J. Yue, and J. Cong, "Using continuum–discontinuum element method to model the foliation-affected fracturing in rock Brazilian test," *Advances in Civil Engineering*, vol. 2021, Article ID 1404568, 9 pages, 2021.

[15] D. Grgic, A. Giraud, and L. Schoumacker, "Dynamic anisotropic elastic properties of a claystone under variable loading direction and saturation," *Geophysical Journal International*, vol. 216, no. 1, pp. 148–163, 2018.

[16] Y. Li, D. Jia, Z. Rui, J. Peng, C. Fu, and J. Zhang, "Evaluation method of rock brittleness based on statistical constitutive relations for rock damage," *Journal of Petroleum Science and Engineering*, vol. 153, pp. 123–132, 2017.

[17] M. S. Masoudian, D. W. Airey, and A. El-Zein, "Experimental investigations on the effect of CO_2 on mechanics of coal," *International Journal of Coal Geology*, vol. 128-129, pp. 12–23, 2014.

[18] J. Pan, Z. Meng, Q. Hou, Y. Ju, and Y. Cao, "Coal strength and Young's modulus related to coal rank, compressional velocity and maceral composition," *Journal of Structural Geology*, vol. 54, pp. 129–135, 2013.

[19] A. Taheri, J. Squires, Z. Meng, and Z. Zhang, "Mechanical properties of brown coal under different loading conditions," *International Journal of Geomechanics*, vol. 17, no. 11, Article ID 06017020, 2017.

[20] R. Zagorščak and H. R. Thomas, "Effects of subcritical and supercritical CO_2 sorption on deformation and failure of high-rank coals," *International Journal of Coal Geology*, vol. 199, pp. 113–123, 2018.

[21] Y. Tang, S. Okubo, J. Xu, and S. Peng, "Study on the progressive failure characteristics of coal in uniaxial and triaxial compression conditions using 3D-digital image correlation," *Energies*, vol. 11, no. 5, Article ID 1215, 2018.

[22] Y. Li, B. Zhao, J. Yang et al., "Experimental study on the influence of confining pressure and bedding angles on mechanical properties in coal," *Minerals*, vol. 12, no. 3, Article ID 345, 2022.

[23] J. Liu, M. Yang, D. Wang, and J. Zhang, "Different bedding loaded coal mechanics properties and acoustic emission," *Environmental Earth Sciences*, vol. 77, Article ID 322, 2018.

[24] L. Tan, T. Ren, X. Yang, and X. He, "A numerical simulation study on mechanical behaviour of coal with bedding planes under coupled static and dynamic load," *International Journal of Mining Science and Technology*, vol. 28, no. 5, pp. 791–797, 2018.

[25] Y.-W. Li, J. Zhang, and Y. Liu, "Effects of loading direction on failure load test results for Brazilian tests on coal rock," *Rock Mechanics and Rock Engineering*, vol. 49, pp. 2173–2180, 2016.

[26] X. Cheng, H. Luan, L. Chen, Y. Jiang, and W. Han, "Numerical investigation on mechanical properties of inhomogeneous coal under uniaxial compression and the role of cleat distribution," *Bulletin of Engineering Geology and the Environment*, vol. 80, pp. 7009–7027, 2021.

[27] Y. Zhao, H. Song, S. Liu, C. Zhang, L. Dou, and A. Cao, "Mechanical anisotropy of coal with considerations of realistic microstructures and external loading directions," *International Journal of Rock Mechanics and Mining Sciences*, vol. 116, pp. 111–121, 2019.

[28] C. Wang, C. Zhang, Y. Li, and C. Zheng, "Numerical investigation of the mechanical properties of coal masses with T-junctions cleat networks under uniaxial compression," *International Journal of Coal Geology*, vol. 202, pp. 128–146, 2019.

[29] H. Chen, Q. Di, W. Zhang, Y. Li, and J. Niu, "Effects of bedding orientation on the failure pattern and acoustic emission activity of shale under uniaxial compression," *Geomechanics and Geophysics for Geo-Energy and Geo-Resources*, vol. 7, 2021.

[30] W. Jiwei, G. Tiankui, C. Ming et al., "Numerical study of the fracture propagation mechanism of staged methane deflagration fracturing for horizontal wells in shale gas reservoirs," *Geoenergy Science and Engineering*, vol. 230, Article ID 212209, 2023.